USING A FAST-GATED CAMERA FOR MEASUREMENTS OF TRANSVERSE BEAM DISTRIBUTIONS AND DAMPING TIMES[*]

M. Minty, R. Brown, F.-J. Decker, P. Emma, P. Krejcik,
T. Limberg, D. McCormick, M. Ross, R. Siemann, and W. Spence
Stanford Linear Accelerator Center
Stanford University, Stanford, California 94309

ABSTRACT

With a fast-gated camera, synchrotron light was used for studying the transverse beam distributions and damping times in the Stanford Linear Collider (SLC) damping rings. By digitizing the image in the camera signal, the turn-by-turn time evolution of the transverse beam distribution was monitored and analyzed. The projections of the digitized image were fit with Gaussian functions to determine the moments of the distribution. Practical applications include the determination of injection matching parameters and the transverse damping times. In this report we describe a synchrotron light monitor and present experimental data obtained in the SLC damping rings.

I. INTRODUCTION

The SLC electron (NDR) and positron (SDR) damping rings reduce the beams' transverse phase space prior to injection into the linear collider. The reduction results from the interplay between the radiated synchrotron light and the energy gain from RF acceleration. If the damping time is short compared to the cycle time, then the extracted beam size is equal to the equilibrium beam size, which depends on the beam energy, the radius of curvature of the design orbit, and the focusing magnet configuration. If the damping time is not small compared to the cycle time, then the extracted beam size depends also on properties of the injected beam, including the injected beam size and lattice matching parameters. For the 1992 SLC production run, the repetition rate was doubled from 60 to 120 Hz, thereby resulting in a cycle time in the NDR comparable to the damping time. To achieve minimum beam sizes and thereby attain higher luminosities, it became essential to monitor the injection parameters and to understand the damping time. These properties may be deduced from measurements of the radiated synchrotron light. In this report we describe the use of fast-gated cameras for studies in the SLC damping rings.

II. GATED CAMERA AND SUPPORT HARDWARE

The gated camera is manufactured by Xybion Electronic Systems Corp.[1] The camera features fast gating capabilities which allow for the imaging of a single bunch on a single revolution. The camera has a dynamic range spanning 12 orders of magnitude with a minimum sensitivity of better than 10^{-6} lux. The camera performance may be optimized by adjusting the intensifier gain, the peak and average light intensity level settings, video gain, and especially the gate width. An internally generated oscillator synchronized signal is provided, or the camera may be synchronized to another camera.

*Presented at the 1992 Accelerator Instrumentation Workshop,
Berkeley, California, October 27–30. 1992.*

Fig. 1. Gated camera intensifier by Xybion[2].

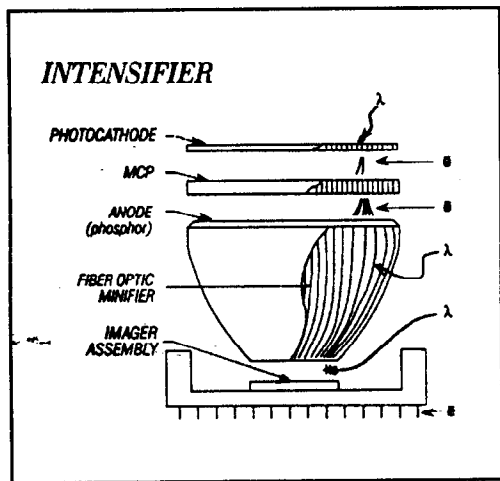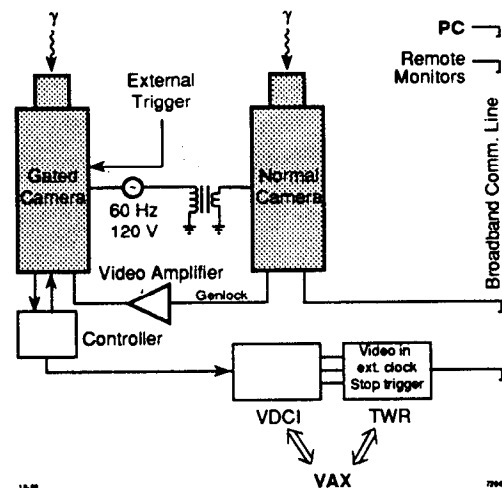Fig. 2. Camera support hardware. The normal camera was used as a beam presence monitor and as a source for synchronization of the gated camera.

Figure 1 shows an overview of the intensifier.[2] It consists of a photocathode that converts the photons to electrons, a multichannel plate (MCP) that amplifies the electron beam signal, a phosphor screen that converts the electrons back into photons, and a fiberoptic minifier that matches the dimension of the screen to an image assembler. The imager (either a CID or CCD array) converts the light energy into a voltage signal to be read out using standard RS–170 time-sequenced format.

In application to the SLC damping rings, we used the ISG–250 model CCD and the GEN2 model gated intensifier with genlock synchronization. The average luminous sensitivity of this intensifier, as determined by the photocathode, ranges from 35 to 45 mA/W over the wavelength range of 500 to 800 nm, and drops off sharply at other wavelengths. The CCD has more than $350,000\ 11 \times 13\ \mu m^2$ pixels that are read out, amplified, and processed to form a composite video signal. With these options, the usable active area of the photocathode is $13 \times 10\ mm^2$ with an image resolution of 400 lines. The gain, which may be ranged from 300 to 18000, was set to near maximum. The camera was remotely triggered with a gate width fixed nominally at the interbunch interval, 60 ns. The trigger timing was adjusted such that the light emitted by a single bunch was centered in the 60 ns gate. The gating of the camera is adjusted by means of an accelerating voltage between the photocathode and the MCP.

Figure 2 shows a block diagram of the apparatus. To remove scrolling resulting from electromagnetic interference (emi), we used a line locked (normal) television camera to supply composite synchronization to the gated camera. The synchronized signal from the normal camera was phase adjusted to offset the emi in the beam image when viewed on a TV monitor. The video amplifier boosted the voltage level of the synchronized signal. The controller adjusted the camera gain and passed the video out signal for processing. We used a SLAC-built video digitizer clock interface (VDCI) and a 30 MHz 8 k×8 bit transient waveform

2

Table 1. Properties of the damping rings and synchrotron light.

| Property	Magnitude	Units
Ring circumference	35.27	m
Beam energy	1.153	GeV
Local bending radius, ρ	2.04	m
Synchrotron radiation energy loss per electron per turn	70	keV
Revolution frequency	8.5	MHz
Number of bunches and current per bunch	2×40	mA
Cycle time in NDR/SDR	8.3/16.6	ms
Critical wavelength, λ_c	10	Å
Opening half-angle at source point, $\alpha = (1/\gamma)\,(\lambda/\lambda_c)^{1/3}$	3.4	mrad

recorder (TWR) as in the automated emittance measurement system.[3] The output signal was piped to a PC or a VAX using a broadband cable.

III. OPTICAL SYSTEM

Some properties of the radiation and operating conditions of the damping rings are summarized in Table 1, and the important optics are shown in Fig. 3. The radiation was extracted from the vacuum chamber using a water cooled, molybdenum mirror. A 1.33 m focal length achromatic lens produced parallel rays for transport to the ceiling of the ring vault and up to an auxilliary building. The long optical path was necessitated by high background radiation levels in the ring vault, and by the desire to have the camera and optics accessible during operation. Distortion of the beam image due to air currents was reduced by blocking the air gap between the light pipe and the penetration walls. Upstairs, the light was focussed with a 1.5 m focal length lens, and split using a pellicle. The reflected light was viewed with a normal camera, which served as a continuous monitor of the beam and a synchronizer for the fast camera. The transmitted beam traversed a fast shutter and a set of adjustable polarizing filters to be viewed using the fast-gated camera. The fast shutter protected the camera from dangerous light levels when data were not being acquired. The location of the image focus was experimentally determined by translating the camera along the optical path to obtain a minimum spot size.

The resolution is dominated by diffraction and depth of focus. The curvature of the particle beam trajectory also contributes to the smallest possible measured beam size. With the polarizers adjusted to pass horizontally polarized light, the diffraction limit was estimated[4] to be 20 μm by evaluation of the Frauenhofer integral.

The depth of field contribution due to the extent of the particle trajectory was estimated using the method of Sabersky.[5] The phase space representation for the light beam produced by a 100 μm rms beam width is plotted in Fig. 4. The curves define the photon beam spatial extent with $\theta(x) = \sqrt{2x/\rho}$. The parallel lines represent the 2 cm aperture defined by the lens located $l = 1.46$ m downstream of the central source point. The contribution to the beam size $\sigma_{r,x}$ is

3
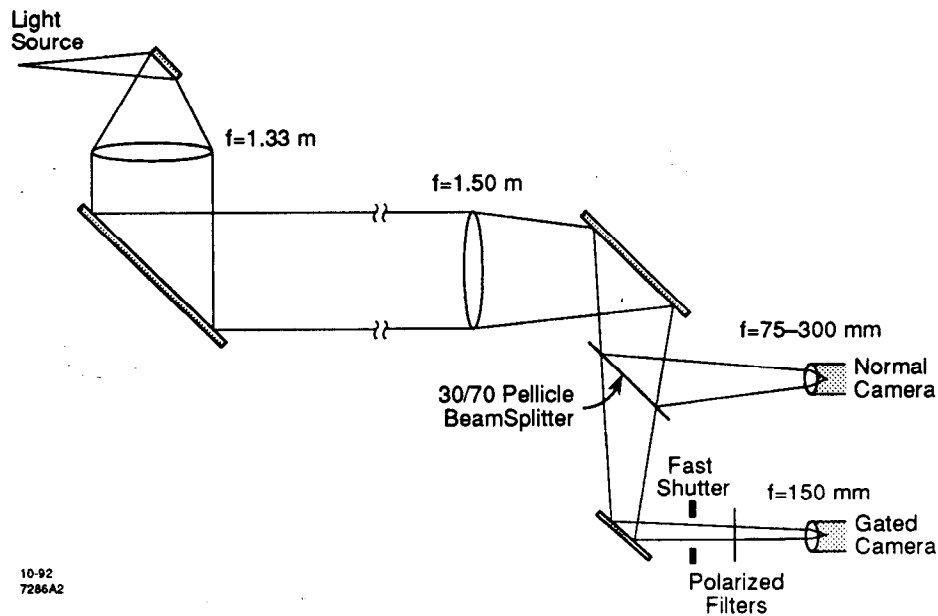
Fig. 3. Light optics. The optics used to produce parallel rays for transport to the cameras is shown. The overview is not to scale.
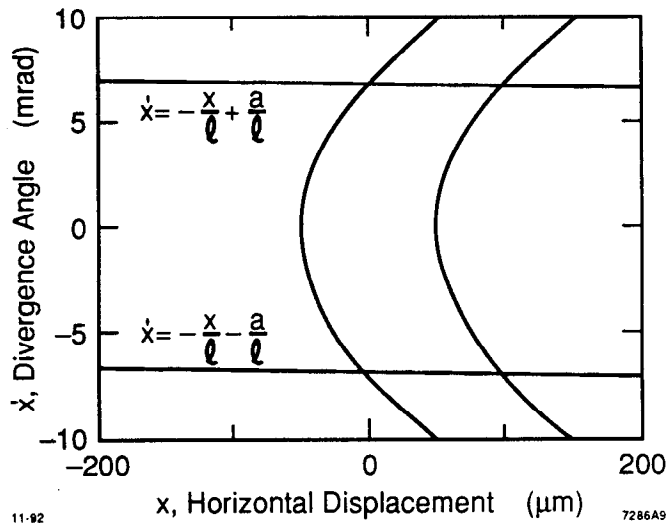
Fig. 4. Photon beam representation. The curves define the edges of the photon beam. The lines represent the horizontal aperture as defined by the geometric optics.

$$\sigma_{r,x}{}^2 = \frac{\int I(x)(x - \bar{x})^2\, dx}{\int I(x)\, dx} \qquad \text{where} \qquad \bar{x} = \frac{\int I(x)x\, dx}{\int I(x)\, dx} \ . \tag{1}$$

and $I(x) \propto \theta(x)$ and the integrals are evaluated from 0 to $a^2\rho/2l^2$. With $a = 1$ cm, $\rho = 2$ m, and $l = 1.46$ m, we estimate a contribution of 15 μm. In the vertical plane, the synchrotron light defines the opening angle, α. The rms contribution to the beam width[6] is $\rho\theta_x\alpha/2.35 = 20$ μm with θ_x the half angle defined by the lens in the horizontal plane. The instrumental resolution was the

4

most difficult to estimate as the system magnification was not carefully controlled. We estimate contributions in x and y of 10 μm. Coupling of the horizontal electron beam size to its energy distribution (dispersion) contributes about 25 μm in x and 30 μm in y with the measured dispersion functions $\eta_x = 3.5$ cm and $\eta_y = 4.0$ cm. Here we assume that the energy spread is equal to the equilibrium fractional energy spread of 7×10^{-4}, which is valid for most of the machine cycle since the longitudinal damping time is about half the transverse damping times. Summing these contributions in quadrature, we find the minimum beam sizes we could expect to measure for these optics are $\sigma_{x,m} = 30$ μm and $\sigma_{y,m} = 40$ μm.

IV. EXPERIMENTAL DATA

In this section we present raw and analyzed data. The raw data showed unexpectedly complicated, yet reproducible, transient particle motion. The analyzed data includes measurements of the transverse damping times and a study of injection transients.

A. Raw data

The video signal from the gated camera was digitized using a personal computer (PC–486) for display on a color monitor. The software was produced by Data Translation[7], and a frame grabber readout scheme was used. Figure 5 shows the images of the transverse profiles of an electron bunch for the first 12 turns. The ring was operated fully betatron-coupled with fractional tunes near quarter integer. The data were obtained by advancing the trigger by one revolution for each snapshot. Successive snapshots correspond to different injection pulses. For a given turn, the beam distribution was observed to be reproducible from pulse-to-pulse. A background image was subtracted from all snapshots, and nearest-neighbor pixel averaging (smoothing) was performed to more clearly distinguish the intensity contours. As can be seen, the beam distribution varied dramatically from turn-to-turn. After the beam filamented (roughly 10 μs), the beam image formed an ellipse.

B. Analyzed data

To obtain quantitative information of the beam distribution, we used a VAX and the SLC control system "correlation plot" facility.[8] The data were processed by first digitizing a background image. Then a beam image was digitized and the background was subtracted. The background-subtracted image was then displayed along with the corresponding projections. The projections were then fit with a Gaussian distribution. Examples of typical online data are shown in Fig. 6, including a three-dimensional digitized image (top) and, from a different bunch passage, projections of the image with Gaussian fits (bottom). The fitting function, which includes a base level offset, was of the form

$$I(z) = a_0 + a_1 \, \exp\left\{-\frac{(z-z_0)^2}{2\sigma_z^2}\right\} \qquad \text{with} \qquad z = x, y \,, \qquad (2)$$

where the fit parameters a_0 are a base level offset, a_1 is the peak amplitude, z_0 is the first moment (mean), and σ_z is the second moment (rms Gaussian beam
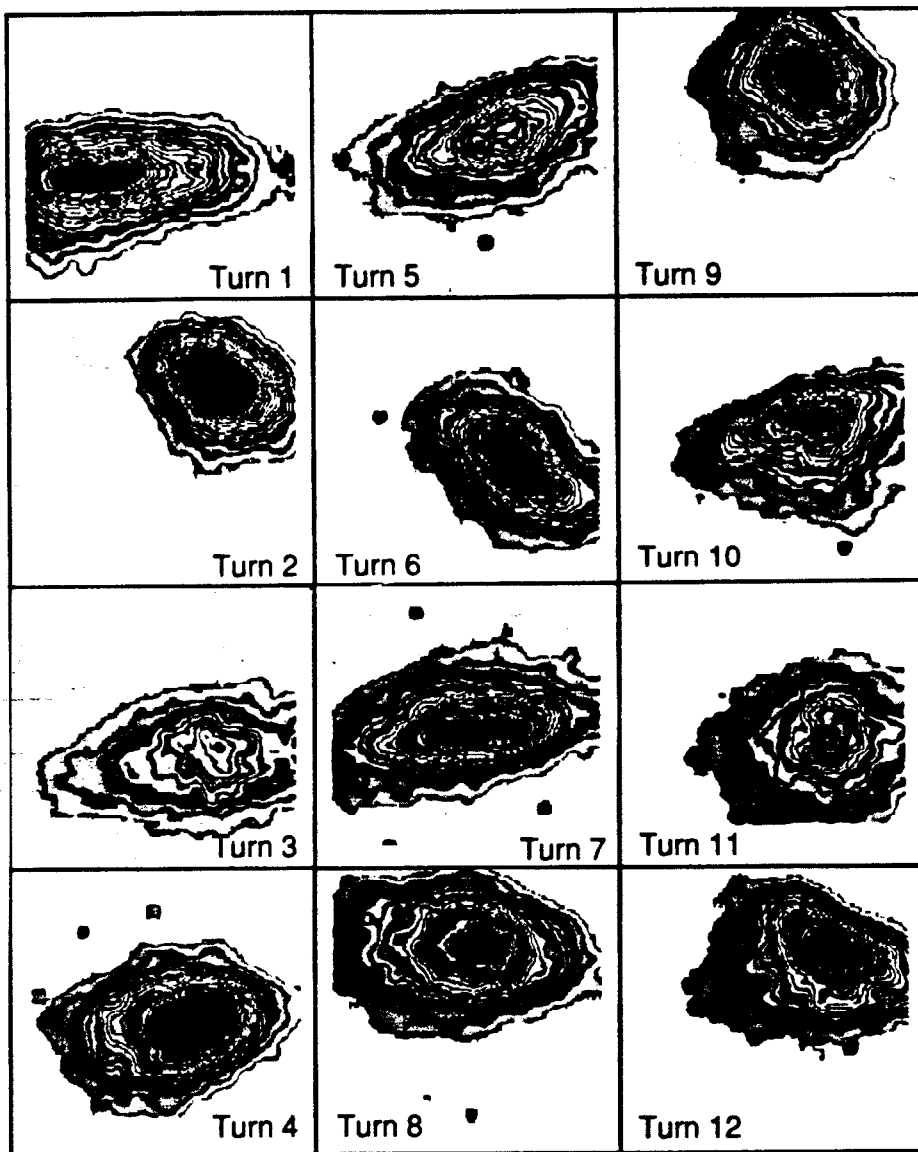
Fig. 5. Twelve turns at injection. For each turn number, a 60 ns gate was used to view the passage of a single bunch. Successive turns correspond to different pulses.

width) of the distribution. In addition, we calculated the area, $A = \int (I(z) - a_0)\, dz$. Nominally, eight images were averaged to reduce the statistical error. The resulting error represented the combined errors from the Gaussian fits and an assumed 2 bit out of 8 bit ADC error. The camera trigger was then advanced through a predetermined set of observation times. For each trigger delay, the data were fit and the results plotted. A plot of the area versus time proved to be especially useful as a diagnostic. Camera saturation, under illumination, and trigger timing errors were diagnosed as a change in an ideally time-independent area curve.
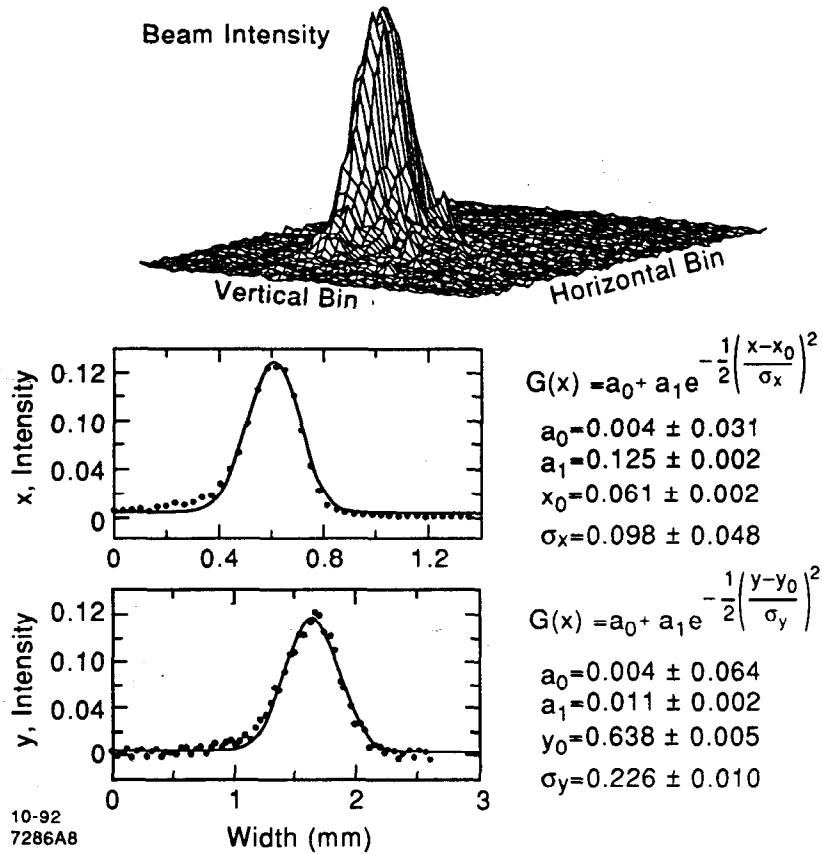
Fig. 6. Gated camera data processed with digitizer. Shown is the three dimensional digitized image (top). Sample projections and Gaussian fits are also shown (bottom).

(i) Transverse damping times

In 1991, the damping times measured with wire scanners downstream of the NDR were longer than expected.[9] The measurements were invasive, tedious, and had possible systematic errors associated with the aperture of the extraction line. Detection of synchrotron light using the gated camera allowed for parasitic and more direct data acquisition.

For a typical damping time measurement, about 50 data points were acquired with eight samples per point. The camera trigger delay was stepped by 0.16 ms. We fitted the measured beam sizes squared $\sigma_j{}^2$, with $j = x, y$ for the damping times τ_j, the injected beam size $\sigma_{i,j}$, and the equilibrium beam size $\sigma_{e,j}$, using the following expression:

$$\sigma_j{}^2 = \sigma_{i,j} \, \exp\left(-\frac{2t}{\tau_j}\right) + \sigma_{e,j}{}^2 \left[1 - \exp\left(-\frac{2t}{\tau_j}\right)\right] . \tag{3}$$

For the graphical display we plotted the linear function $\ell n(\sigma_j{}^2 - \sigma_{e,j}^2)$. Results for the damping times in the two transverse planes of the NDR are shown in Fig. 7. The measured damping times were 4.11 ± 0.11 ms in x (left) and 4.50 ± 0.12 ms in y (right).

7

$\sigma_x^2 - \sigma_{e,x}^2$ (mm^2) $\sigma_y^2 - \sigma_{e,y}^2$ (mm^2)

$$\sigma_x^2 = \sigma_{ix}^2(1-e^{-2t/\tau_x}) + \sigma_{ex}^2 e^{-2t/\tau_x}$$

$$\sigma_y^2 = \sigma_{iy}^2(1-e^{-2t/\tau_y}) + \sigma_{ey}^2 e^{-2t/\tau_y}$$

$\sigma_{iy}^2 = 0.3540 \pm 0.0066$
$\sigma_{ey}^2 = 0.0488 \pm 0.0012$
$\chi^2/DF = 0.943$

$\tau_x = 4.11 \pm 0.11$

$\sigma_{ix}^2 = 0.0716 \pm 0.0013$
$\sigma_{ex}^2 = 0.0100 \pm 0.0003$
$\chi^2/DF = 0.741$

$\tau_y = 4.50 \pm 0.12$
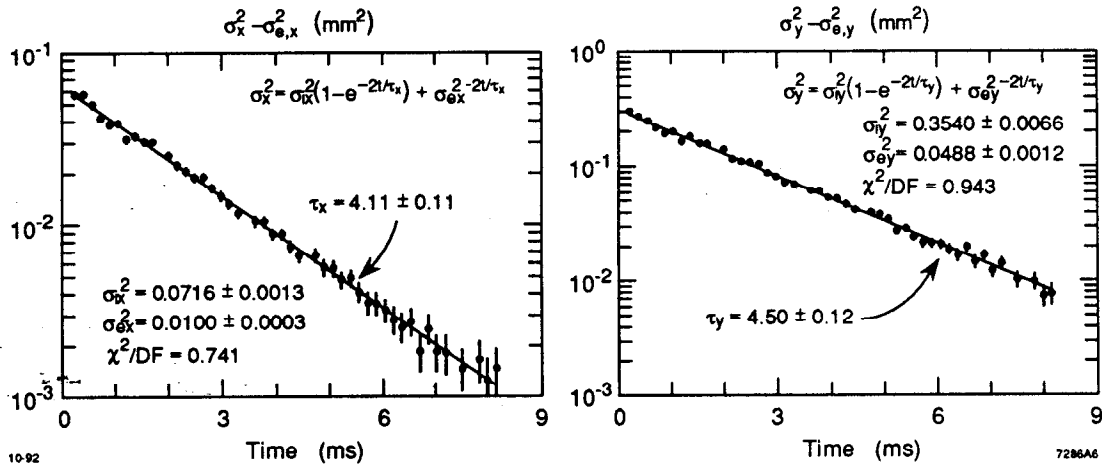
Time (ms) Time (ms)

10-92   7286A6

Fig. 7. Damping time data in NDR taken before circumference adjustment. On the left is plotted the data for the x plane, and on the right, the data for the y plane.

In the SDR, synchrotron light emitted from positrons was also detected. The magnet configuration and the optical systems in the NDR and SDR were nominally identical. In the SDR, however, the measured damping times were 3.69 ± 0.26 ms in x and 3.85 ± 0.15 ms in y. This discrepancy motivated an adjustment in the NDR circumference; specifically, the ring arc magnet centers were moved outward, while the orbit length determined by the locked (to the linac) RF frequency was held fixed. After the realignment, the damping times were again measured as shown in Fig. 8, and found to be 3.41 ± 0.09 ms in x and 3.90 ± 0.09 ms in y. This corresponds to a 15% reduction in the average damping time, which is consistent with the measured change in circumference. The extracted beam emittance, however, did not decrease accordingly. Comparison of Figs. 7 and 8 show that the injected beam size increased.

$\sigma_x^2 - \sigma_{e,x}^2$ (mm^2) $\sigma_y^2 - \sigma_{e,y}^2$ (mm^2)

$$\sigma_x^2 = \sigma_{ix}^2(1-e^{-2t/\tau_x}) + \sigma_{ex}^2 e^{-2t/\tau_x}$$

$\sigma_{ix}^2 = 0.1400 \pm 0.0045$
$\sigma_{ex}^2 = 0.0087 \pm 0.0003$
$\chi^2/DF = 0.234$

$$\sigma_y^2 = \sigma_{iy}^2(1-e^{-2t/\tau_y}) + \sigma_{ey}^2 e^{-2t/\tau_y}$$

$\sigma_{iy}^2 = 0.6560 \pm 0.0185$
$\sigma_{ey}^2 = 0.0034 \pm 0.0014$
$\chi^2/DF = 0.431$

$\tau_x = 3.41 \pm 0.09$

$\tau_y = 3.90 \pm 0.09$

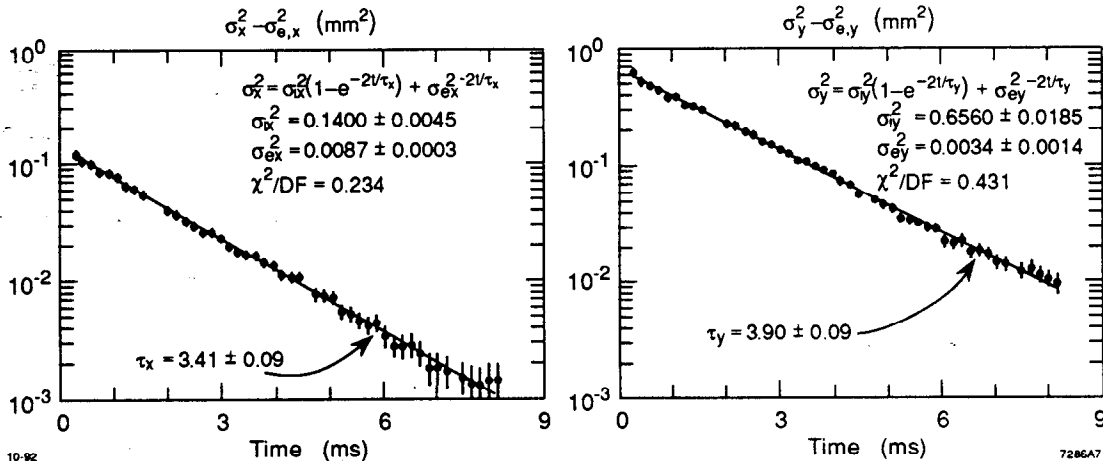Time (ms) Time (ms)

10-92   7286A7

Fig. 8. Damping time data in NDR taken after circumference adjustment. On the left is plotted the data for the x plane and on the right is plotted the data for the y plane.

(ii) Injection transients

In a separate series of measurements, transverse phase space matching was studied by stepping the trigger time by a single revolution (117.647 ns) for the
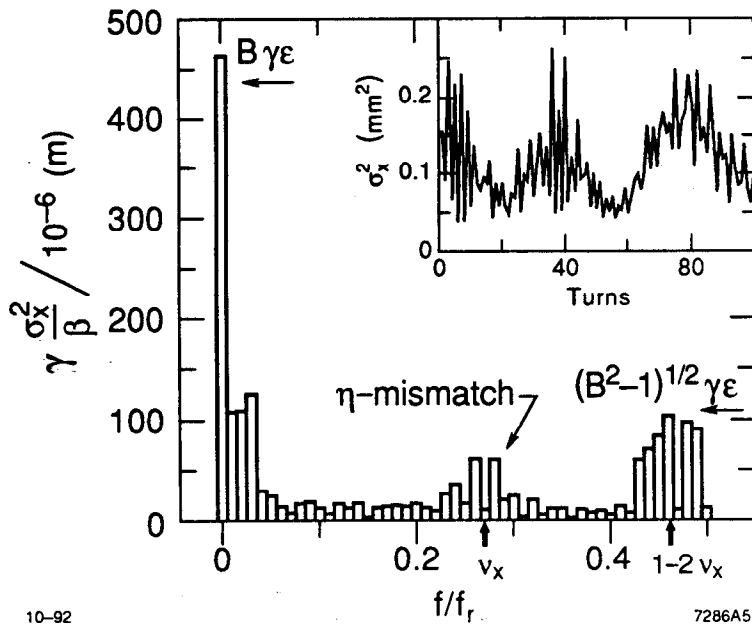
Fig. 9. The mean square beam width, $\sigma_x{}^2$, for the first 100 turns after injection (insert) and the corresponding Fourier transform normalized by the periodic, or "matched," betatron function. The fractional horizontal β tune was $\nu_x = 0.27$.

first few hundred consecutive turns. Samples were digitized, and the x and y plane projections were fit to Gaussians. This yielded accurate second moments despite the fact that the injected x–y distribution was evidently more complicated than bi-Gaussian. The second moment time series was then Fourier transformed (Fig. 9) to exhibit peaks at the betatron frequency and at its second harmonic, indicating the presence and size of dispersion and β–mismatches (respectively) in the injected beam. Combining the measured heights of the zero frequency and the ν_x peaks allowed separation of the β–mismatch factor B from the emittance ϵ. The phase of the mismatch was also obtained. In principle, simultaneous sampling from more than one location in the ring can be used to separately determine the energy spread and the injected dispersion function.[10] The observation of higher betatron harmonics, e.g., $3\nu_x$, would indicate the presence of nonlinearities in the lattice of the ring and provide a measure of their strength.

(iii) Absolute emittance

The system resolution has so far not entered curicially in the data presented. In the damping time measurement the contribution to the beam size due to resolution cancelled, and in the injection transient study the beam size at injection was much larger than the resolution. A least-squares fit was made to beam size (σ) measured with the gated camera, and to beam emittance (ϵ) measured with wire-scanners in the linear accelerator downstream of the damping ring. The extraction time t_e was varied from 0.50 to 8.33 ms in eight steps. The fitting function was

$$\sigma_z{}^2(t_e) = c_{1,z}\,\epsilon(t_e) + c_{2,z} \qquad \text{with} \qquad z = x, y \ .$$

9

Here $c_{1,z}$ contains information about the β functions at the source point, and $c_{2,z} = \sigma_{z,m}{}^2$ with $\sigma_{z,m}$ containing contributions from resolution and dispersion (see Sec. III). From the fit, we obtained $\sigma_{x,m} = (69 \pm 18)$ μm and $\sigma_{y,m} = (113 \pm 19)$ μm, which are larger than our estimates from Sec. III. Possible explanations include distortions in the optical path (for example, mirror degradation in the vacuum chamber), changes in the optical properties of the lenses (for example, the light intensity was observed over a period of months to change), or emittance blowup in the extraction line.

V. CONCLUSIONS

Use of the fast-gated camera for detecting synchrotron light has proven to be invaluable in understanding the transverse beam dynamics at the SLC damping rings. The short gate width allowed for the imaging of the passage of a single bunch. By adjusting the camera trigger time, injection transients and transverse damping times were studied. The damping times were accurately measured and then reduced by predicted adjustments to the ring circumference. In the future, we hope to gain a better understanding of the injection transients in order to better control injection errors. In addition, we plan to upgrade the existing synchrotron light facilities to allow for the continous monitoring of the beam size and damping times in both rings.

REFERENCES

1. Gated Camera, Xybion Corp., San Diego, CA 92126.
2. Reproduced with permission from Xybion Corp.
3. M. C. Ross et al , "Automated Emittance Measurements in the SLC," 1987 IEEE Part. Accel. Conf., Washington, D.C., p. 725.
4. A. Hofmann and F.'Meòt, "Optical Resolution of Beam Cross-Section Measurements by Means of Synchrotron Radiation," Nucl. Instrum. and Methods **203**, 483 (1982); J. D. Jackson, *Classical Electrodynamics,* (John Wiley and Sons, Inc., NY, 1975).
5. A. P. Sabersky, "The Geometry and Optics of Synchrotron Radiation", Part. Accel. **5**, 199 (1973).
6. R. Littauer, "Beam Instrumentation", Proc. Physics of High Energy Particle Accelerators, Stanford, 1982 .
7. Data Translation, Marlboro, MA.
8. L. Hendrickson et al., "Correlation Plot Facility in the SLC Control System," Int. Conf. on Accel. and Large Experimental Physics Control Systems, Tsukuba, Japan, 1991.
9. F.-J. Decker et al.,"Measured Emittance versus Store Time in the SLC Damping Ring," 1992 European Part. Accel. Conf., Berlin, Germany, p. 342; T. Limberg et al., "Calculations of Emittance and Damping Time Effects in the SLC Damping Rings," ibid., p. 682.
10. N. Merminga et al., "Transverse Phase Space in the Presence of Dispersion," 1991 IEEE Part. Accel. Conf., San Francisco, p. 461.